*Proc. Natl. Acad. Sci. USA*
Vol. 84, pp. 4283–4287, June 1987
Medical Sciences

# Quantitative studies of human cardiac metabolism by $^{31}P$ rotating-frame NMR

(myocardial energetics/rotating-frame spectroscopic imaging)

MARTIN J. BLACKLEDGE*, BHEESHMA RAJAGOPALAN, ROLF D. OBERHAENSLI, NICHOLAS M. BOLAS, PETER STYLES, AND GEORGE K. RADDA

Medical Research Council Clinical Magnetic Resonance Facility, John Radcliffe Hospital, Headington, Oxford OX3 9DU, United Kingdom

*Communicated by Britton Chance, March 6, 1987*

**ABSTRACT** **We have developed $^{31}P$ NMR spectroscopic methods to determine quantitatively relative levels of phosphorous-containing metabolites in the human myocardium. We have used localization techniques based on the rotating-frame imaging experiment and carried out with a double-surface coil probe. Information is obtained from selected slices by rotating-frame depth selection and from a complete one-dimensional spectroscopic image using phase-modulated rotating-frame imaging. The methods collect biochemical information from metabolites in human heart, and we use the fact that the phosphocreatine/ATP molar ratio in skeletal muscle at rest is higher than that in working heart to demonstrate that localization has been achieved for each investigation. The phosphocreatine/ATP molar ratio in normal human heart has been measured as 1.55 ± 0.20 (mean ± SD) (3.5-sec interpulse delay) in six subjects using depth selection and as 1.53 ± 0.25 (mean ± SD) in four subjects using spectroscopic imaging. Measurement of this ratio is expected to give a useful and reproducible index of myocardial energetics in normal and pathological states.**

It has been shown that $^{31}P$ NMR spectroscopy provides a useful insight into myocardial energetics using isolated and perfused rat hearts (1–3). In particular, the relative concentrations of phosphocreatine (PCr), ATP, and $P_i$, as well as intracellular pH, can yield information about the relationship between ATP supply and demand and give insight into metabolic control. It has also been shown that $^{31}P$ NMR spectra from the hearts of live rats were qualitatively similar to those of the isolated perfused organ, but differed quantitatively in that the PCr/ATP molar ratio was 30% higher *in vivo* than for the isolated heart (4). A similarly high PCr/ATP molar ratio of 1.7 was observed in the canine heart, by using a catheter coil, which removed the necessity for surgery (5).

The first spectroscopic investigation of human heart was performed on infants, where localization was achieved by simply using a surface coil probe. A PCr/ATP molar ratio of 2.0 ± 0.1 was reported in a healthy 18-month-old child compared to a lower value of 1.3 in an 8-month-old child with cardiomegaly (6). In contrast, using depth-resolved spectroscopy, the PCr/ATP molar ratio was found to be 1.3 ± 0.4 in a single adult (7). Accurate, rapid, and reproducible measurements of PCr/ATP ratio will be essential in the investigation of human heart disease by $^{31}P$ NMR. The development of differential localization techniques have made such measurements theoretically possible in human subjects (8–12).

The specific problems associated with investigating the human heart using $^{31}P$ NMR include the achievement of adequate spatial localization and establishment of objective criteria to ensure that the data obtained are representative of cardiac muscle. Any contamination by a signal from overlying skeletal muscle will distort the measured PCr/ATP ratio, as studies show that this ratio in skeletal muscle is very different from that in cardiac muscle (13, 14). In the present study, we have used rotating-frame depth selection (15–17) with a double-concentric surface coil probe (18, 19, and P.S., referred to as a personal communication in ref. 20) to localize the signal from flat, planar, disc-shaped slices at a series of distances into the chest. The relative intensities of PCr and ATP confirm the position of the slice within the chest.

We have also used phase-modulated rotating-frame imaging (PMRFI) to create a one-dimensional spectroscopic image of the chemical shift and distance representing a map of planar, sensitive discs at various distances from the surface of the chest. We have used a technique (21) to remove the "phase twist" incurred in the two-dimensional data set to produce high-resolution spectral images with no dispersive component.

In studies of human heart, localization has been achieved using a switched, $B_0$ gradient localization method (7) or static-field profiling method (9). In contrast, we use the inherent biochemistry of the sample (specifically the PCr/ATP molar ratio) to provide evidence of localization. Our techniques have proved reliable and reproducible, and it is now possible to investigate the cardiac metabolism of patients with heart disease.

## METHODS

**Localization Strategy.** The heart lies directly below two skeletal muscles, the intercostal and the transversus thoracis. A slice-selection experiment is, therefore, particularly appropriate for localizing the signal from the heart and eliminating the signal from the overlying skeletal muscle. The subject lies prone, such that the probe covers the position of the apex and anterior wall of the heart that has previously been estimated from a two-dimensional echo cardiogram of the subject's chest. The probe used is a double-concentric surface coil with a transmitter 15 cm in diameter and a receiver 6.5 cm in diameter that is offset forward of the transmitter plane by 2 cm (18, 19, and P.S., referred to as a personal communication in ref. 20). This coil configuration ensures that to a first-order approximation the reception region is localized to the linear region of the transmitter gradient and that off-axis effects due to the curvature of the transmitter field are negligible because of the much-reduced receiver sensitivity at these points. The validity of these approximations has been verified by extensive phantom experiments (19) and confirmed by computer simulation of phase and amplitude information carried out by Garwood *et al.* (22).

The publication costs of this article were defrayed in part by page charge payment. This article must therefore be hereby marked "*advertisement*" in accordance with 18 U.S.C. §1734 solely to indicate this fact.

Abbreviations: PCr, phosphocreatine; PMRFI, phase-modulated rotating-frame imaging.

*To whom reprint requests should be addressed.

The region of interest is, therefore, centered on the anterior wall of the left ventricle and encompasses the left ventricular apex and parts of the right ventricle. When using rotating-frame depth selection, the signal is collected from discs, ≈6 cm in diameter and ≈2 cm wide, at various depths into the chest. Data from each slice takes either 3 or 6 min to acquire. Alternatively, we collect a one-dimensional image consisting of a series of discs, 5 mm wide, at various distances from the surface of the chest. In this case the whole data set takes 35 min to acquire. The discs interrogated are smaller laterally than the heart, so that there is no contamination from lung or skeletal muscle at the same depth. As depth increases, the slices contain more heart and less skeletal muscle, and the PCr/ATP molar ratio falls until a plateau is reached when skeletal muscle no longer contaminates the slice and the spectrum is purely from heart. As the slice goes through the heart wall (≈1-cm thick in the left ventricle) and into the blood in the ventricle, the PCr/ATP molar ratio stays constant but the signal/noise ratio falls.

**Rotating-Frame Methods.** We have used two methods of localization based on the rotating-frame imaging experiment (21, 23). Both experiments rely on a gradient $B_1$ excitation field in which spins experience a "flip angle" dependent on their position in the $B_1$ field strength and the length of the transmitter pulse. The magnetization vectors of spins in different field strengths nutate about the $x'$-axis of the rotating frame at different frequencies ($f_1$) with respect to pulse width. This frequency can be used to characterize the $B_1$ field strength at that point. Our double-surface coil probe provides a relatively linear $B_1$ gradient and so the nutational frequency is inversely proportional to depth.

(i) *Depth Selection.* We can utilize the nutational frequency ($f_1$) distribution to localize signal from a region in a particular $B_1$, field strength, by applying a series of pulses that maximally excite this region.

$$\theta = (2n + 1)(\pi/2)(-1)^n \qquad (n = 0, 1, 2, \ldots). \qquad [1]$$

Combination of the data files resulting from each pulse width will achieve positive coherence of the signal over a slice of the $B_1$ field gradient, rendering this slice sensitive. There is destructive interference of the signal from elsewhere in the $B_1$ gradient, and the signal cancels.

We define the selected region to be Gaussian shaped in the $B_1$ field direction by acquiring a signal at four different pulse lengths. The sequence is designed so that the addition of the data files effectively reduces the detection region to a slice. The sequence of pulses applied is given as follows: 20 pulses at $\theta_{\pi/2}$, 14 pulses at $-3\theta_{\pi/2}$, 5 pulses at $5\theta_{\pi/2}$, and 1 pulse at $-7\theta_{\pi/2}$. In this way we can receive a signal from a 6-cm disc, of 2 cm in width, at a position defined by the length of the pulses.

(ii) *PMRFI.* Rotating-frame imaging enables signal to be collected from all of the sample within the sensitive region of the receiver coil. A set of free induction decays is collected, the observation pulse width being incremented for each successive data accumulation. The nutational frequency at which the spin vector precesses assigns the position of the spin in the $B_1$ gradient. A two-dimensional Fourier transform of the data matrix produces a map of distance and chemical shift, representing spectra from a series of planar discs at various depths from the probe. This method (amplitude-modulated rotating-frame imaging) is inherently insensitive because the magnetization vector precesses at $f_1$ about the $x'$-axis of the rotating frame with respect to the incremental observation pulse, so that of the two components ($y'$ and $z'$), only the $y'$ component is detected. The $z'$ component, being aligned with the magnetic field $B_0$, is undetected. To make use of all of the information present (21), we can transfer the magnetization vector into the $x'$–$y'$ plane, immediately after the incremental pulse, using a $\pi/2$ pulse applied along the $y'$-axis (Fig. 1). Now, the signal is no longer amplitude modulated. All the available signal is acquired after each increment, and the signal is phase modulated; i.e., the relative amount of $x'$ and $y'$ magnetization varies with pulse angle. A second Fourier transform (*FT*) with respect to incremental pulse width, then decodes the $f_1$ phase frequencies to give spatial position. The data are then presented as a two-dimensional matrix of chemical shift and distance.

The PMRFI experiment has three advantages. First, there is an improvement of sensitivity of $\sqrt{2}$. Second, as all the magnetization is in the $x'$–$y'$ plane at the end of the pulse sequence, relaxation due to $T_1$ always commences from the same point, and so there is no spatial distortion due to partial saturation effects (19). Third, the harmonic subtraction from high flux regions that is encountered in the depth selection is removed in the imaging experiment.

With our double coil we detect a signal from a region equal to ≈0.2–0.8 of the transmitter coil radius away from the surface. Over this region the $B_1$ field strength varies from ≈0.5–1.5 of the midgradient value. Therefore, the nominal

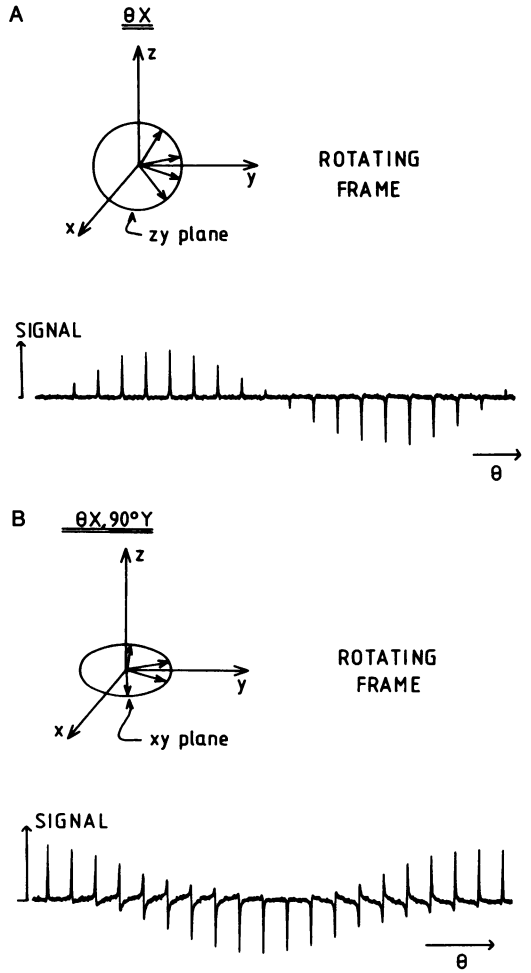


FIG. 1. The amplitude and PMRFI experiments. (*A*) In the amplitude modulated experiment, the observation pulse $\theta_x$ is incremented, thus modulating the amplitude of the observed signal. In the rotating frame this corresponds to the detection only of the $y$ component of the magnetization vector. The $z$ component is aligned along the $B_0$ axis and is, therefore, undetectable. (*B*) The application of a $\pi/2_{+y}$ pulse immediately after the incremental pulse to "flip" the magnetization from the $y$–$z$ plane into the $x$–$y$ plane renders both components measurable. The modulation is now that of relative $x$ and $y$ components of the measured magnetization; i.e., the data are phase-modulated with respect to the incremental pulse width.

90° pulse is effective in transferring the $z$ component of the magnetization onto the $x'$-axis to an accuracy of ≥70% in the receiver region. The inaccuracy produces some amplitude modulation (≈15%) of received signal from the front and back of the sample. We chose a simple $\pi/2$ at the center of the sample region as a phase-encoding pulse. This was used in preference to composite pulses designed to be effective in transferring all of the magnetization into the $x'$–$y'$ plane, because studies we conducted to model the magnetization vector response show that, in the required range of transmitter field strength ($B_1$) and resonance offset ($B_0$), the amplitude and phase were retained optimally by the simple pulse. The imperfection of the pulse causes some signal loss, with an artifactual signal appearing in the quadrature image in $f_1$.

The phase modulation of signal leads to a known artifact of two-dimensional NMR; this is a phase twist induced in the final matrix that originates in the mixing of real and imaginary $f_0$ data after application of a quadrature $f_1$ transform with respect to pulse width. This is because both the real and imaginary data, before the $f_1$ transform, have absorption and dispersion mode components and a mixed absorption and dispersion mode data set results from the second transform. In order that no phase twist occurs after the second transform, the data set should contain only absorption- and no dispersion-mode signal. Otherwise the dispersive component broadens the lines in both dimensions as well as making the spectra impossible to phase.

This phase twist can be removed by repeating the experiment but applying a $-x$ incremental pulse instead of a $+x$ pulse, thus mixing the $x$ and $y$ components of the magnetization in the opposite sense. The frequency of precession ($f_1$) in the rotating frame also has the opposite sign. The two data sets are processed identically except that after the second transform, the $-x$ data set is reversed about the origin in $f_1$ (thus reversing the sign of $f_1$ again) and then added to the matrix resulting from the $+x$ experiment. This cancels the dispersive component of the signal, removing the broad dephasing artifact in $f_0$ and $f_1$, and adds the absorption-mode signal. This is equivalent in theory to applying a conjugate Fourier transform to the $-x$ data set and subtracting the data sets as described by Hoult (21) but is easier to execute using standard two-dimensional software. The process is illustrated in Fig. 2. Attention is drawn to the improvement in spatial resolution that results from elimination of dispersive signals.

The PMRFI pulse sequence is given by

$$\theta_{\pm x} - \theta_{\pi/2(+y)} - AQ - T. \qquad [2]$$

The PMRFI spectroscopic imaging has been applied to the localization of human heart to give high-resolution spectra *in vivo* in about 35 min. Data were collected using 24 incremental pulse widths. The repetition rate for the study of heart was 3.5 sec.

## RESULTS AND DISCUSSION

An example of a series of 3-min depth-selection accumulations representing slices from the human chest is shown in Fig. 3*A*. The PCr/ATP ratio reaches a plateau as depth increases and signal from the 2,3-bisphosphoglycerate in the blood in the heart increases as we examine deeper regions. The 2,3-bisphosphoglycerate signal consists of two peaks that, at a blood pH of 7.4, appear at 5.4 ppm and at 6.2 ppm (24). It has, therefore, not been possible to resolve an inorganic phosphate peak in the human heart, thus making the measurement of intracellular pH impossible. There is also a large peak in the phosphodiester region of the spectrum that appears as we receive signal from the heart.

A plot of the PCr/ATP molar ratio versus depth is shown in Fig. 3*B*. As depth increases, this ratio decreases and then reaches a plateau. The fact that the PCr/ATP ratio is a constant over this region confirms that the spectra are not

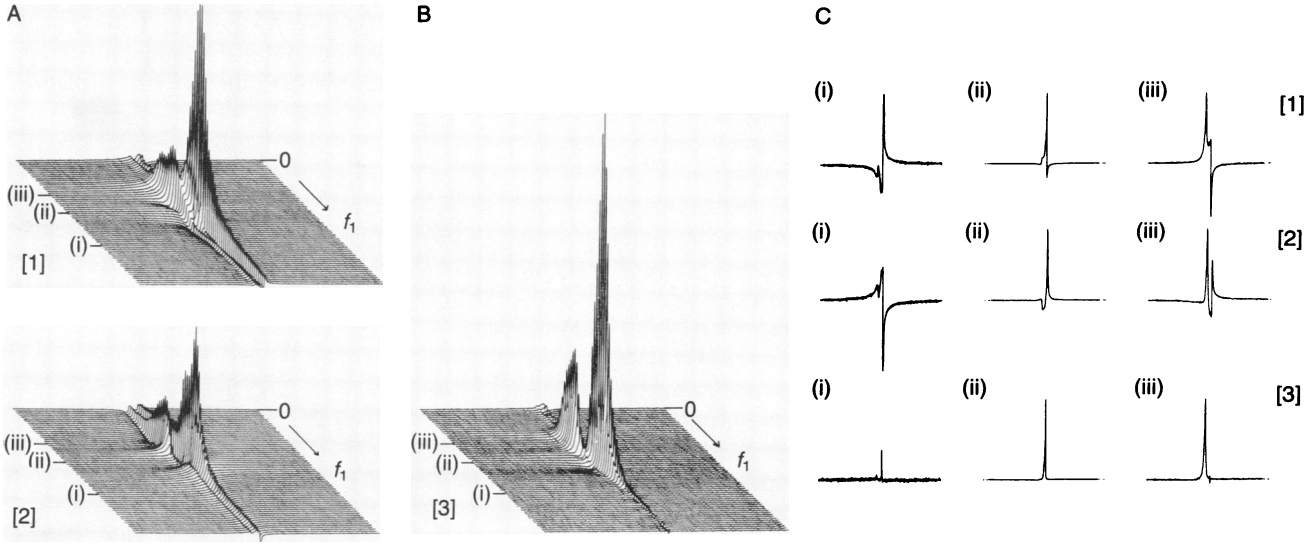


FIG. 2. The elimination of the phase twist due to mixing the real and imaginary $f_0$ data in the second ($f_1$) transform. (*A*) The data set resulting from a two-dimensional phase Fourier transform of a PMRFI experiment carried out on a two-compartment phantom (compartment dimensions, 2 cm in depth × 10 cm in diameter), containing phosphates at two chemical shifts. The phantom was placed such that the compartments lay sequentially in the $B_1$ field gradient, the $y$-axis represents the spatial dimension ($f_1$). These data were acquired from 30 incremental pulse widths. No line broadening was applied in either dimension. The incremental pulse had phase $+x$, and the phase-encoding pulse had the phase $+y$ in the case of data set 1. Data set 2 represents the identical experiment except that the phase of the incremental pulse was $-x$ and that the data set has been reversed about the $f_1 = 0$ origin. Notice that the phase twist is reversed in sense in this case. (*B*) The final PMRFI data set 3, resulting from data set 1 added directly to data set 2. The dispersive phase twist has been removed completely, and the absorption-mode signal remains. The data, therefore, retain the maximum resolution in both dimensions. (*C*) Spectra selected from three equivalent positions *i*, *ii*, and *iii* throughout data sets 1, 2, and 3, as shown in *A* and *B*. In data set 3, the broad dispersive wings in $f_1$ and $f_0$ disappear, and the resultant spectra are absorption mode only. Spectrum *ii* represents localization of the right-hand compartment, whereas spectrum *iii* represents localization of the left-hand compartment.

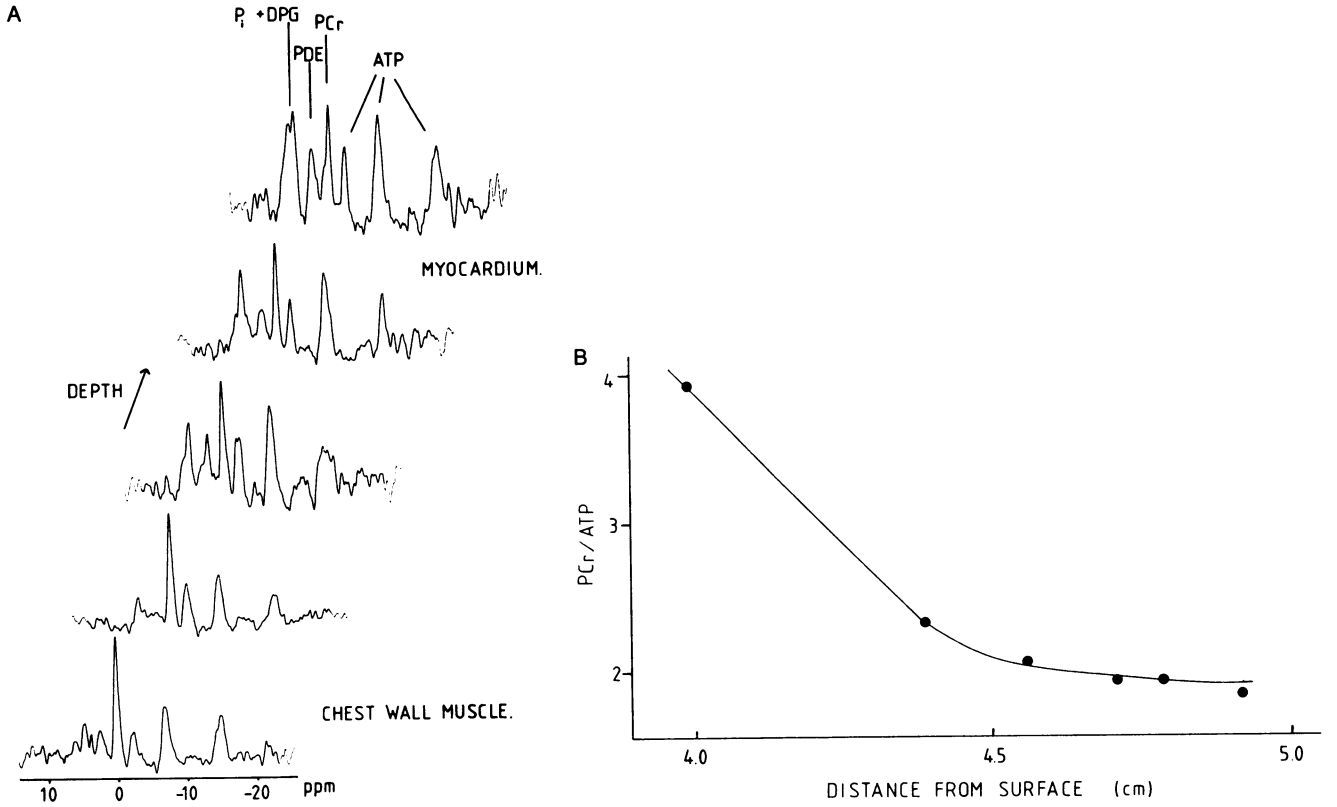


FIG. 3. Rotating-frame depth-selection heart spectra. (*A*) $^{31}$P NMR spectra from a series of slices acquired at increasing depths into the chest. DPG, bisphosphoglycerate; PDE, phosphodiester. (*B*) A plot of the PCr/γ-ATP molar ratio of the series shown in *A*. The data were processed by 15-Hz exponential multiplication and quantitated by triangulation of the peaks. The carrier frequency is between PCr and γ-ATP.

contaminated by signal from skeletal muscle. This plateau contains two valuable pieces of information; first, the PCr/ATP ratio in heart muscle and, second, the position of the heart with respect to pulse width. The method is, therefore, internally calibrated for each investigation and for the anatomy of each subject.

The pulse-angle dependence of the method allows one to calibrate the distance from phantom studies, although this assumes that the transmitter tuning does not change dramatically from phantom to subject. An exact real space calibration is not essential in each study, the essential factor is that the depth increases with pulse width and that a plateau is

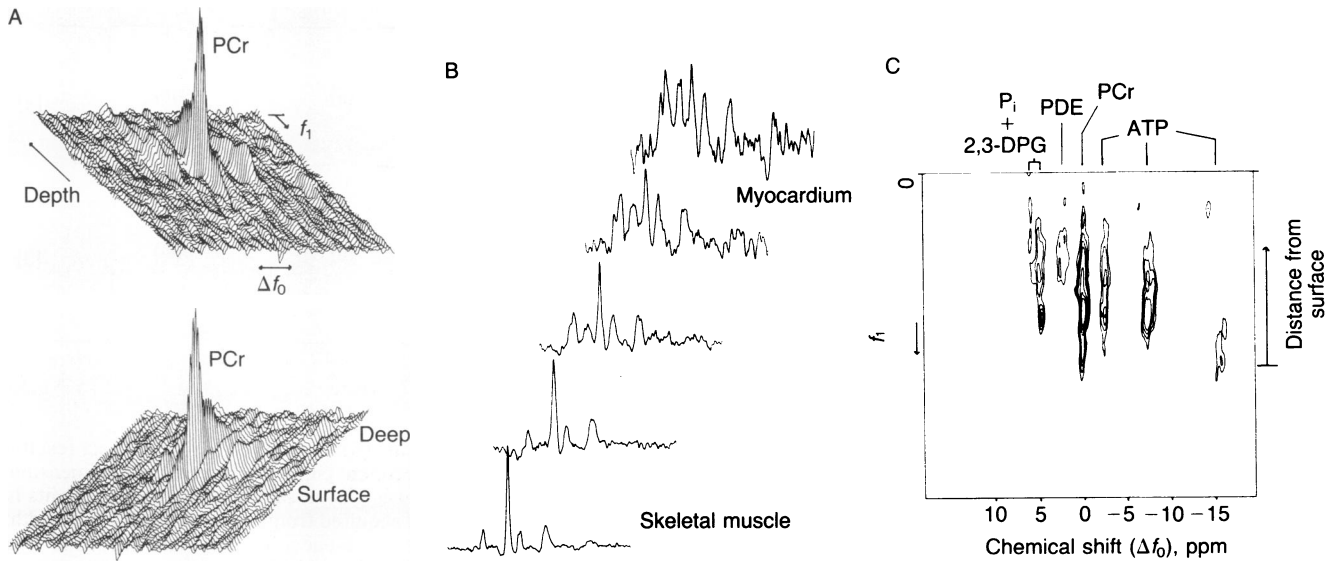


FIG. 4. Phase-modulated rotating-frame spectroscopic image of human heart. (*A*) The stackplot of a two-dimensional PMRFI image of the human heart and overlying skeletal muscle. Distance appears along the *y*-axis. A 15-Hz line broadening was applied in the $f_0$ dimension; none was applied in the $f_1$ dimension. Spectra are plotted from both projections to display the whole data set. (*B*) Spectra selected from the image in *A*; the superficial slices represent skeletal muscle, whereas the deeper slices emanate from the heart. These data were collected in 35 min. Spatial resolution was ≈5 mm. (*C*) Contour plot of the same data set, the *y*-axis represents the spatial dimension, and the *x*-axis represents the chemical shift. 2,3-DPG, 2,3-bisphosphoglycerate; PDE, phosphodiester.

reached. It is worth noting that the method makes no assumptions about the PCr/ATP ratio except that it is different from resting skeletal muscle and that it is constant throughout the myocardium we examine.

There is no PCr signal from blood in the ventricle (24), and the signal from ATP in blood is negligible, so this has no detectable effect on the measured ratio as we acquire slices containing blood.

We have chosen an interpulse delay of 3.5 sec to reduce the possibility of distortion of the sensitive profile due to $T_1$ effects (19). This gives a PCr/ATP ratio in normal heart muscle of 1.55 ± 0.20 (mean ± SD) in six individuals. In one subject, studied five times, the measured PCr/ATP ratio was 1.80 ± 0.20 (mean ± SD).

An image acquired using PMRFI is shown in Fig. 4. Distance from coil appears along the *y*-axis of this plot. The superficial slices are from skeletal muscle, while the deeper slices represent heart. We can examine signal from different regions of the sample by selecting spectra from different parts of the image (Fig. 4*B*). Again a plot of the PCr/ATP ratio against increasing distance for this experiment reaches a plateau at 1.6, which is in very good agreement with the value obtained from a slice selection experiment that we carried out on the same subject. In four subjects, we have measured a PCr/ATP ratio of 1.53 ± 0.25 using the PMRFI. This method has better spatial resolution than the depth-selection protocol (the resolution is ≈5 mm). The values of the PCr/ATP ratio obtained for the adult human myocardium are very close to those reported for animal hearts *in vivo* (4, 5).

We realize that without cardiac cycle gating, the values represent an average over all cycles of the heart. Both the methods reported here have off-resonance effects (19) resulting in a spatial and amplitude distortion of peaks far from resonance. This is defined by the available rf power amplifier (150 W). This artifact can be reduced by using higher transmitter power. In practice, 1 kW would reduce the artifacts to a negligible level for $^{31}P$ spectral width at 2 tesla. In this study all PCr/ATP ratios are measured with respect to γ-ATP where there is a negligible off-resonance problem.

## CONCLUSION

We have shown that we can obtain good quality spectra from the human heart using rotating-frame methods with a double-coil probe system. Both experiments can be carried out in an acceptable experimental time for patient investigation. The methods are internally calibrated with a technique that relies on the available biochemistry of the interrogated muscle. This is used to provide the necessary evidence that we are studying the pure myocardium. We have thus measured the PCr/ATP ratio in human heart muscle. At this stage we cannot derive intracellular pH measurements from the data.

In the way we have performed this study, the imaging experiment has better resolution, at the expense of more complex data processing. The usefulness of the PCr/ATP molar ratio as an index of myocardial energetics has been shown in pathological states in a study in infants (25). We believe that this ratio can be measured in adults using the techniques described here. It may be possible to optimize the spatial resolution by gating the acquisition to the cycle of the heart, although we have not yet investigated the possible advantages of cardiac or respiratory gating. We are aware that in the event of an inhomogeneous metabolism within the heart wall, the results may be difficult to interpret. These techniques are, therefore, particularly suitable for the investigation of cardiomyopathies or general heart disorders as the planar localization matches the relevant heart anatomy.

This work was supported by the Medical Research Council of Great Britain, the British Heart Foundation, the Department of Health and Social Security, and Grant HL-18708 from the National Institutes of Health. R.D.O. is the recipient of a grant of the Swiss National Science Foundation.

1. Gadian, D. G., Hoult, D. I., Radda, G. K., Seeley, P. J., Chance, B. & Barlow, C. (1976) *Proc. Natl. Acad. Sci. USA* **73,** 4446–4448.
2. Garlick, P. B., Radda, G. K., Seeley, P. J. & Chance, B. (1977) *Biochem. Biophys. Res. Commun.* **77,** 1256–1262.
3. Jacobus, W. E., Taylor, G. J. N., Hollis, D. P. & Nunally, R. C. (1977) *Nature (London)* **265,** 756–758.
4. Grove, T. H., Ackerman, J. J. H., Radda, G. K. & Bore, P. J. (1980) *Proc. Natl. Acad. Sci. USA* **77,** 299–302.
5. Kantor, H. L., Briggs, R. W. & Balaban, R. S. (1984) *Circ. Res.* **55,** 261–266.
6. Whitman, G. J. R., Chance, B., Bode, H., Maris, J., Haselgrove, J., Kelley, R., Clark, B. J. & Harken, A. H. (1985) *J. Am. Coll. Cardiol.* **5,** 745–749.
7. Bottomley, P. A. (1985) *Science* **229,** 769–772.
8. Gordon, R. E., Hanley, P. E., Shaw, D., Gadian, D. G. & Radda, G. K. (1980) *Nature (London)* **287,** 736–738.
9. Oberhaensli, R. D., Galloway, G., Hilton-Jones, D., Styles, P., Bore, P., Rajagopalan, B., Taylor, D. & Radda, G. K. (1987) *Br. J. Rad.*, in press.
10. Ordidge, R. J., Connelly, A. & Lohman, J. A. B. (1986) *J. Magn. Reson.* **66,** 283–294.
11. Styles, P., Scott, C. A. & Radda, G. K. (1985) *Magn. Reson. Med.* **2,** 402–409.
12. Bottomley, P. A., Foster, T. B. & Darrow, R. D. (1984) *J. Magn. Reson.* **59,** 338–342.
13. Radda, G. K. (1986) *Science* **233,** 640–645.
14. Taylor, D. J., Bore, P. J., Styles, P., Gadian, D. G. & Radda, G. K. (1983) *Mol. Biol. Med.* **1,** 77–94.
15. Metz, K. R. & Briggs, R. W. (1985) *J. Magn. Reson.* **64,** 172–176.
16. Garwood, M., Schleich, T., Ross, B. D., Matson, G. B. & Winters, W. D. (1985) *J. Magn. Reson.* **65,** 239–251.
17. Styles, P., Galloway, G., Blackledge, M. & Radda, G. K. (1986) *Proc. 4th Annual Meeting Soc. Magn. Reson. Med.*, London, 1985 (Soc. Magn. Reson. Med.), pp. 422–423.
18. Styles, P. S., Smith, M. B., Briggs, R. W. & Radda, G. K. (1985) *J. Magn. Reson.* **62,** 397–405.
19. Blackledge, M. J., Styles, P. & Radda, G. K. (1987) *J. Magn. Reson.* **71,** 246–258.
20. Bendall, M. R., Connelly, A. & McKendry, J. M. (1986) *Magn. Reson. Med.* **3,** 157–163.
21. Hoult, D. I. (1979) *J. Magn. Reson.* **33,** 183–197.
22. Garwood, M., Schleich, T., Bendall, M. R. & Ugurbil, K. (1987) *Proc. 5th Annual Meeting Soc. Magn. Reson. Med.*, Montreal, 1986 (Soc. Magn. Reson. Med.), pp. 850–851 (abstr.).
23. Cox, S. J. & Styles, P. (1980) *J. Magn. Reson.* **40,** 209–212.
24. Moon, R. B. & Richards, J. H. (1973) *J. Biol. Chem.* **248,** 7276–7278.
25. Clark, B., Gewitz, M., Schnall, M., Subramanian, H., Kelly, R., Leigh, J. S., Egan, J., Maris, J., Hilberman, M. & Chance, B. (1986) *Proc. 2nd World Congr.*, eds. Doyle, E. F., Engle, M. A., Gersonay, W. M., Rashkind, W. J. & Talmer, N. S. (Springer, Berlin), pp. 211–214.